

⁵¹V Solid-State Magic Angle Spinning NMR Spectroscopy of Vanadium Chloroperoxidase

Neela Pooransingh-Margolis,[†] Rokus Renirie,[‡] Zulfiqar Hasan,[‡] Ron Wever,[‡]
Alexander J. Vega,[†] and Tatyana Polenova^{*,†}

Contribution from the Brown Laboratories, Department of Chemistry and Biochemistry,
University of Delaware, Newark, Delaware 19716, Van 't Hoff Institute for Molecular Sciences,
Faculty of Science, University of Amsterdam, NieuweAchtergracht 129,
1018 WS Amsterdam, The Netherlands

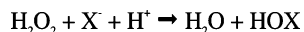
Received January 20, 2006; E-mail: tpolenov@chem.udel.edu

Abstract: We report ⁵¹V solid-state NMR spectroscopy of the 67.5-kDa vanadium chloroperoxidase, at 14.1 T. We demonstrate that, despite the low concentration of vanadium sites in the protein (one per molecule, 1 μmol of vanadium spins in the entire sample), the spinning sideband manifold spanning the central and the satellite transitions is readily detectable. The quadrupolar and chemical shift anisotropy tensors have been determined by numerical simulations of the spinning sideband envelopes and the line shapes of the individual spinning sidebands corresponding to the central transition. The observed quadrupolar coupling constant C_Q of 10.5 ± 1.5 MHz and chemical shift anisotropy δ_σ of -520 ± 13 ppm are sensitive reporters of the geometric and electronic structure of the vanadium center. Density functional theory calculations of the NMR spectroscopic observables for an extensive series of active site models indicate that the vanadate cofactor is most likely anionic with one axial hydroxo- group and an equatorial plane consisting of one hydroxo- and two oxo- groups. The work reported in this manuscript is the first example of ⁵¹V solid-state NMR spectroscopy applied to probe the vanadium center in a protein directly. This approach yields the detailed coordination environment of the metal unavailable from other experimental measurements and is expected to be generally applicable for studies of diamagnetic vanadium sites in metalloproteins.

Introduction

Vanadium haloperoxidases (VHPO) catalyze a two-electron oxidation of halide to hypohalous acid in the presence of hydrogen peroxide; the native enzymes require diamagnetic V(V) for their activity (Scheme 1).

Scheme 1. The Reaction Catalyzed by Vanadium Haloperoxidases



Haloperoxidases are named after the most electronegative halide they are able to oxidize (i.e., chloroperoxidases oxidize Cl^- , Br^- , and I^-). These enzymes are universally present in marine algae, terrestrial fungi, and in some lichen; they are thought to be involved in the biosynthesis of halogenated natural products.^{1–3} The kinetics and mechanism of haloperoxidases have been the subject of multiple studies^{4,5} due to their potential

applications in industrial-scale biocatalytic conversions: vanadium haloperoxidases are the most efficient halide oxidants known to date.²

Despite the wealth of experimental data about vanadium haloperoxidases, many aspects of their function and mechanism are unclear, in part due to the fact that the enzymes are colorless and diamagnetic in their active form, hampering spectroscopic studies. Weak UV bands were detected in the region 300–330 nm that report on vanadate binding to VCPO;⁶ this has been to date the only spectroscopic probe to study the individual steps in the mechanism. The factors governing the substrate specificity, i.e., whether a particular enzyme will or will not display chlorinating activity, are not understood.^{7–9} The primary amino acid sequences are conserved to only ca. 20% across the various families of vanadium haloperoxidases.^{10,11} The overall structures of these proteins were also found to be different with the exception of the regions in the vicinity of the active site.^{10–12}

[†] University of Delaware.

[‡] University of Amsterdam.

- (1) Vollenbroek, E. G. M.; Simons, L. H.; Van Schijndel, J. W. P. M.; Barnett, P.; Balzar, M.; Dekker, H.; Vanderlinden, C.; Wever, R. *Biochem. Soc. Trans.* **1995**, *23* (2), 267–271.
- (2) Butler, A. *Coord. Chem. Rev.* **1999**, *187*, 17–35.
- (3) Butler, A. *Science* **1998**, *281*, 207–210.
- (4) Van Schijndel, J. W. P. M.; Barnett, P.; Roelse, J.; Vollenbroek, E. G. M.; Wever, R. *Eur. J. Biochem.* **1994**, *225* (1), 151–157.
- (5) Macedo-Ribeiro, S.; Hemrika, W.; Renirie, R.; Wever, R.; Messerschmidt, A. *J. Biol. Inorg. Chem.* **1999**, *4*, 209–219.

- (6) Renirie, R.; Hemrika, W.; Piersma, S. R.; Wever, R. *Biochemistry* **2000**, *39*, 1133–1141.
- (7) Wever, R.; Hemrika, W. Vanadium Haloperoxidases. In *Handbook of Metalloproteins*; Messerschmidt, A., Huber, R., Poulos, T., Wiegardt, K., Eds.; John Wiley & Sons, Ltd.: Chichester, 2001; Vol. 1, pp 1417–1428.
- (8) Renirie, R.; Hemrika, W.; Wever, R. *J. Biol. Chem.* **2000**, *275* (16), 11650–11657.
- (9) Murphy, C. D. *J. Appl. Microbiol.* **2003**, *94*, 539–548.
- (10) Weyand, M.; Hecht, H. J.; Kiess, M.; Liaud, M. F.; Vilter, H.; Schomburg, D. *J. Mol. Biol.* **1999**, *293* (3), 595–611.
- (11) Messerschmidt, A.; Wever, R. *Proc. Natl. Acad. Sci. U.S.A.* **1996**, *93*, 392–396.

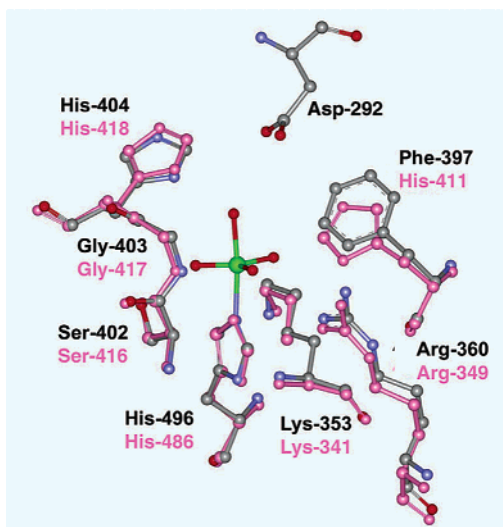


Figure 1. Active sites of VCPO from *C. inaequalis* (CPK color) and VBPO from *A. nodosum* (pink) have been superimposed to demonstrate the similar geometries. Active site residue labels correspond to VCPO (top) and VBPO (bottom). The proposed vanadate geometry consists of an axial hydroxo group trans to His-496/His-486 and three equatorial oxo ligands. At a pH lower than 8.0 protonation of one of the oxo groups may occur. The figure has been prepared using the original pdb coordinates (pdb codes 1idq and 1qj9) in DSViewer Pro (Accelrys, Inc.)

On the other hand, the amino acids lining the first and the second hydrogen-bonding spheres for the vanadate active site are highly conserved with one exception: a Phe residue in chloroperoxidases is invariably substituted by a His residue in bromoperoxidases. The active sites' geometries of the chloro- and bromoperoxidase are found to be very similar,¹⁰ as illustrated in Figure 1. Mutation studies suggest that the electrostatic potential distribution changes are detrimental to the chlorinating activity in a series of mutant chloroperoxidases, yet the crystal structures for a number of these mutants reveal intact or nearly intact conformation of the active site.^{6,8,13} Thus, a delicate balance of multiple interactions between the active site residues has been proposed to be responsible for the chlorinating activity of the haloperoxidases,⁸ a hypothesis that remains to be corroborated.

The X-ray crystal structure determined at pH 8.0 revealed that, in the resting state of VCPO, the vanadate cofactor is covalently bound to the N ϵ 2 atom of a histidine residue (His-496 in the VCPO from *C. inaequalis*). The negative charge of the vanadate group is compensated by hydrogen bonds to several positively charged protein sidechains (Lys-353, Arg-360, and Arg-490).¹¹ Ser-402 and Gly-403 form hydrogen bonds with the equatorial oxygens of the vanadate cofactor; an additional hydrogen bond may exist between the axial hydroxo group and His-404. However, the presence and positions of hydrogen atoms could not be unambiguously determined from the crystal structure due to the inherently limited resolution; therefore, the nature of the vanadium first coordination sphere ligands (i.e., whether a particular group is oxo- or hydroxo-) still remains the subject of debate.

Recently, the first quantum mechanical calculations of the electronic structure and geometry of the vanadium center in the resting state^{14,15} and peroxo forms^{15,16} of a series of VHPO active

site models were reported. Several interesting conclusions were drawn. In the resting state, at least one equatorial oxygen needs to be protonated to stabilize the metal cofactor. The axially bound hydroxide proposed from the X-ray crystallographic data results in a low energy structure; however, axially bound water is also energetically favorable. Curiously, the calculations suggest that the protonation state of the vanadate ion is likely to be greater than previously proposed.¹⁴

Following this study, hybrid quantum mechanical/molecular mechanics (QM/MM) calculations were performed by Carlson, Pecoraro, and Kravitz on very large VCPO active site models.¹⁷ In addition to the 8 active site residues treated quantum mechanically, 433 residues and 24 structural water molecules were included in the calculation and described with molecular mechanics. This exciting work highlighted the pivotal role of the protein environment in creating the long-range electrostatic field necessary for the stabilization of the resting state. A hybrid resting state consisting of the two lowest-energy minima has been proposed. Anionic vanadate with one axial and one equatorial hydroxo group was found to be nearly isoenergetic with the anionic vanadate containing an axial water ligand. The roles of the individual amino acid residues and of the oxo atoms of the cofactor have been re-examined, leading to a revised catalytic cycle.

Therefore, the mutagenesis and computational results in aggregate suggest that the electronic structure of the vanadate cofactor is modulated both by the protein and by the coordinated water or hydroxide ligands. However, the lack of direct spectroscopic probes has so far prevented gaining further insight on the electronic environment of the vanadium center intimately related to the enzymatic mechanism of vanadium haloperoxidases.

In this work, we introduce ⁵¹V solid-state NMR spectroscopy as a direct and sensitive reporter of the vanadium site in vanadium chloroperoxidases (VCPO). ⁵¹V is a half-integer quadrupolar nucleus ($I = 7/2$) with high natural abundance (99.8%) and relatively high gyromagnetic ratio (Larmor frequency of 157.6 MHz at 14.1 T). The dominant anisotropic quadrupolar and chemical shielding interactions are directly observed in the solid-state NMR spectra and bear a wealth of information about the geometric and electronic structure of the vanadium site.^{18–20} We demonstrate that the sensitivity of the NMR experiments in vanadium chloroperoxidase is such that both tensorial interactions are readily extracted from the numerical simulations of the spinning sideband (ssb) envelopes and the central transition ssb lineshapes. The ⁵¹V spectra reveal large quadrupolar interaction at the vanadium center providing the first direct experimental evidence of the asymmetric electronic charge distribution at the metal site. Density functional theory (DFT) calculations of the NMR parameters conducted

(12) Isupov, M. N.; Dalby, A. R.; Brindley, A. A.; Izumi, Y.; Tanabe, T.; Murshudov, G. N.; Littlechild, J. A. *J. Mol. Biol.* **2000**, *299* (4), 235–249.
 (13) Tanaka, N.; Hasan, Z.; Wever, R. *Inorg. Chim. Acta* **2003**, *356*, 288–296.

(14) Zampella, G.; Kravitz, J. Y.; Webster, C. E.; Fantucci, P.; Hall, M. B.; Carlson, H. A.; Pecoraro, V. L.; De Gioia, L. *Inorg. Chem.* **2004**, *43* (14), 4127–4136.
 (15) Borowski, T.; Szczepanik, W.; Chruszcz, M.; Broclawik, E. *Int. J. Quantum Chem.* **2004**, *99* (5), 864–875.
 (16) Zampella, G.; Fantucci, P.; Pecoraro, V. L.; De Gioia, L. *J. Am. Chem. Soc.* **2005**, *127* (3), 953–960.
 (17) Kravitz, J. Y.; Pecoraro, V. L.; Carlson, H. A. *J. Chem. Theory Comput.* **2005**, *1* (6), 1265–1274.
 (18) Skibsted, J.; Nielsen, N. C.; Bildsøe, H.; Jacobsen, H. J. *Chem. Phys. Lett.* **1992**, *188*, 405–412.
 (19) Pooransingh, N.; Pomerantseva, E.; Ebel, M.; Jantzen, S.; Rehder, D.; Polenova, T. *Inorg. Chem.* **2003**, *42*, 1256–1266.
 (20) Lapina, O. B.; Shubin, A. A.; Khabibulin, D. F.; Terskikh, V. V.; Bodart, P. R.; Amoureux, J. P. *Catal. Today* **2003**, *78* (1–4), 91–104.

in this work for an extensive number of active site models previously addressed by Carlson, Pecoraro, De Gioia and co-workers¹⁴ in conjunction with the experimental NMR results indicate that the vanadate cofactor is most likely anionic with the hydroxo group in the axial position and the equatorial plane composed of one hydroxo and two oxo groups. Our results are in remarkable agreement with the conclusions drawn from the computational studies by the above authors^{14,17} and, furthermore, permit us to rule out the additional plausible energetically favorable structures as described in detail below.

Theoretical Background: ⁵¹V Solid-State NMR Spectroscopy

For half-integer spin nuclei, such as ⁵¹V, the solid-state NMR spectra are dominated by a combination of the quadrupolar interaction (the interaction between the electric quadrupole moment of the nucleus and the electric field gradient on the nuclear site) and nuclear magnetic shielding anisotropy. The latter is observable in the NMR spectra via the symmetric part of the chemical shift anisotropy (CSA) tensor (refs 18, 21 and references therein). The different magnitudes and different symmetry properties of the quadrupolar and chemical shift anisotropies allow these tensorial quantities to be extracted from a single solid-state NMR spectrum, along with the mutual orientations of the quadrupolar and CSA tensors.^{18,19,22,23} In contrast, the anisotropic components of the tensorial interactions are averaged out in solution, resulting in a loss of valuable electronic and geometric information and detection of only the isotropic chemical shifts by solution NMR spectroscopy.

The total Hamiltonian in addition includes the dipolar and the radio frequency terms and can be expressed as

$$H = H_{Zeeman} + H_{RF} + H_{DIP} + H_Q + H_{CSA} \quad (1)$$

The first three terms represent the Zeeman, the radio frequency field, and the dipolar interactions. The dipolar interaction is generally much smaller than the quadrupolar and magnetic shielding anisotropy and will be omitted in the subsequent discussions. The last two terms are the quadrupolar and CSA interactions, which dictate the spectral shape. They are conveniently expressed in a spherical tensor notation in terms of the spatial (R_{mn}) and spin (T_{mn}) variables:²⁴

$$H_Q^{(1)} = \frac{eQ}{4S(2S-1)} R_{20}^Q T_{20}^S = \omega_Q [3S_z^2 - S(S+1)] \quad (2)$$

$$H_Q^{(2)} = \frac{C_Q}{\omega_0} \sum_{m \neq 0} \frac{R_{2m} R_{2-m} [T_{2m}, T_{2-m}]}{2m} \quad (3)$$

$$H_{CSA} = -\gamma(R_{00}^{CS} T_{00}^S + R_{20}^{CS} T_{20}^S) = (\omega_{CS}^{iso} + \omega_{CS}^{aniso}) S_z \quad (4)$$

$H_Q^{(1)}$ and $H_Q^{(2)}$ are the first- and second-order quadrupolar interactions. The quadrupolar and CSA tensor elements are defined in a spherical harmonics basis set according to the standard notation.^{25,26}

- (21) Smith, M. E.; van Eck, E. R. H. *Prog. Nucl. Magn. Reson. Spectrosc.* **1999**, *34*, 159–201.
 (22) Huang, W.; Todaro, L.; Francesconi, L. C.; Polenova, T. *J. Am. Chem. Soc.* **2003**, *125* (19), 5928–5938.
 (23) Huang, W. L.; Todaro, L.; Yap, G. P. A.; Beer, R.; Francesconi, L. C.; Polenova, T. *J. Am. Chem. Soc.* **2004**, *126* (37), 11564–11573.
 (24) Frydman, L. *Annu. Rev. Phys. Chem.* **2001**, *52*, 463–498.
 (25) Cohen, M. H.; Reif, F. *Solid State Phys.* **1957**, *5*, 321–438.

$$C_Q = \frac{eQV_{zz}}{h}; \eta_Q = \frac{V_{yy} - V_{xx}}{V_{zz}} \quad (5)$$

$$\delta_\sigma = \delta_{zz} - \delta_{iso}; \eta_\sigma = \frac{\delta_{yy} - \delta_{xx}}{\delta_{zz} - \delta_{iso}}; \delta_{iso} = 1/3(\delta_{xx} + \delta_{yy} + \delta_{zz}) \quad (6)$$

where C_Q is the quadrupolar coupling constant (in MHz); V_{xx} , V_{yy} , V_{zz} are the principal components of the electric field gradient (EFG) tensor, with $V_{zz} = eq$ being its largest principal component, and $|V_{zz}| \geq |V_{yy}| \geq |V_{xx}|$. C_Q defines the overall breadth of the spectral envelope. Q is the vanadium quadrupole moment (-0.052×10^{-28} V/m²);²¹ e is the electronic charge; h is the Planck constant. Haeberlen–Mehring–Spiess convention is followed in the definition of the CSA tensor: δ_{iso} is the isotropic chemical shift; δ_{xx} , δ_{yy} , and δ_{zz} are the principal components of the CSA tensor. δ_σ is the reduced anisotropy of the CSA tensor determining the breadth of the tensor (throughout the text, we will refer to δ_σ as anisotropy). Note that, according to Haeberlen–Mehring–Spiess, anisotropy of the CSA tensor is defined as $\Delta\delta = \delta_{zz} - (\delta_{xx} + \delta_{yy})/2$. We also note that the chemical shift anisotropy tensor is related to the chemical shielding anisotropy tensor as follows:²⁷

$$\hat{\delta} = \hat{I}\sigma_{iso} - \hat{\sigma} \quad (7)$$

where $\hat{\delta}$ is the chemical shift tensor, $\hat{\sigma}$ is the chemical shielding tensor, \hat{I} is the unit matrix, and σ_{iso} is the isotropic value of the chemical shielding of the reference compound, VOCl₃.

η_Q and η_σ are the asymmetry parameters of the EFG and CSA tensors, defining the deviations from axial symmetry.

Upon spinning the solid powder sample at the magic angle (54.7°) the spectral broadening due to the second-rank spatial components R_{20} of tensorial anisotropies of $H_Q^{(1)}$ and H_{CSA} is efficiently averaged into a spinning sideband pattern, while the fourth-rank terms of the $H_Q^{(2)}$, since they are partially preserved, give rise to characteristic second-order line shapes. It has been demonstrated by Skibsted, Nielsen, Jacobsen and their colleagues as well as in our recent work that the ⁵¹V quadrupolar and the chemical-shielding tensors, and their relative orientations, can be extracted with high precision by detecting the complete manifold of spinning sidebands from the central and the satellite transitions and subsequently comparing the experimental and the simulated spectra.^{18,19,22,23,28–35} These tensorial interactions can be further correlated with the structure and electronic properties at the vanadium site by classical electrostatic calculations for ionic compounds^{22,23} or more generally via the density functional theory (DFT).^{19,36,37} In this work, we

- (26) Sandstrom, D.; Hong, M.; Schmidt-Rohr, K. *Chem. Phys. Lett.* **1999**, *300* (1–2), 213–220.
 (27) Facelli, J. C. *Concepts Magn. Reson., Part A* **2004**, *20* (1), 42–69.
 (28) Bak, M.; Rasmussen, J. T.; Nielsen, N. C. *J. Magn. Reson.* **2000**, *147*, 296–330.
 (29) Nielsen, U. G.; Jacobsen, H. J.; Skibsted, J. *Inorg. Chem.* **2000**, *39*, 2135–2145.
 (30) Nielsen, U. G.; Jacobsen, H. J.; Skibsted, J. *J. Phys. Chem. B* **2001**, *105*, 420–429.
 (31) Skibsted, J.; Jacobsen, C. J. H.; Jacobsen, H. J. *Inorg. Chem.* **1998**, *37*, 3083–3092.
 (32) Skibsted, J.; Nielsen, N. C.; Bildsøe, H.; Jacobsen, H. J. *J. Magn. Reson.* **1991**, *95*, 88–117.
 (33) Fyfe, C. A.; zu Altenschildesche, H. M.; Skibsted, J. *Inorg. Chem.* **1999**, *38*, 84–92.
 (34) Skibsted, J.; Jacobsen, H. J. *Inorg. Chem.* **1999**, *38*, 1806–1813.
 (35) Jacobsen, H. J.; Skibsted, J.; Bildsøe, H.; Nielsen, N. C. *J. Magn. Reson.* **1989**, *85*, 173–180.

employ the quantum mechanical DFT approach to interpret the experimental NMR spectroscopic observables.

Experimental Section

Materials and Methods. All chemicals were purchased from either Sigma or Fisher, unless otherwise specified.

Expression and Purification of Vanadium Chloroperoxidase. Vanadium chloroperoxidase from *Curvularia inaequalis* was isolated and purified using the recombinant system in *Saccharomyces cerevisiae*, as described by Hemrika et al.³⁸ A modification to the original procedure was made to minimize sodium salts during purification, to eliminate possible sources of ²³Na, as the presence of the latter could potentially interfere with the detection of ⁵¹V because of the similar gyromagnetic ratios and resonance frequencies for the two isotopes.

The yeast cells were inoculated in a starter culture containing 0.17% (w/v) yeast nitrogen base (without amino acids and ammonium sulfate), 0.5% (w/v) ammonium sulfate, leucine (36 μg/mL), tryptophan (24 μg/mL), and 2% (w/v) glucose and were grown to the end of the log phase, after which the culture was transferred to media containing 1% (w/v) yeast extract, 2% (w/v) peptone, and 1% (w/v) glucose. The culture was grown until the end of the log phase. Induction was carried out using galactose to a final concentration of 4%. The culture was grown for three more days.

The yeast cells were harvested by centrifugation at (35 min × 3800 rpm), followed by resuspension in 50 mM TrisSO₄, pH 8.3. Release of the protein from the cells was achieved by sonication on ice, and removal of cell debris was done by further centrifugation. DNA precipitation was achieved by the addition of 2-propanol to the supernatant, followed by centrifugation (30 min × 15 000 rpm). The supernatant was then added to DEAE Sephacel resin that was washed and pre-equilibrated in 50 mM TrisSO₄, pH 8.3. The protein was allowed to bind to the resin by continuous stirring for 2 h, after which the resin was poured into a column. The resin was then washed with 2 column volumes of 0.1 M KCl in 50 mM TrisSO₄, pH 8.3 followed by protein elution using 0.6 M KCl in 50 mM TrisSO₄, pH 8.3.

Prior to further purification by FPLC, the protein was dialyzed against 25 mM piperazine HCl, pH 5.5, containing 100 μM sodium orthovanadate, followed by centrifugation (30 min × 15 000 rpm, 4 °C) to remove any excess DNA. The protein was loaded onto a MonoQ column at a rate of 0.5 mL/min. The column was then washed with 2 column volumes of 25 mM piperazine HCl, pH 5.5 to remove any unbound material. Protein elution was achieved by applying a linear salt gradient, using 2 M KCl in 25 mM piperazine HCl, pH 5.5. The protein eluted between 0.12 M to 0.15 M KCl. The active fractions were pooled, sodium orthovanadate was added to a final concentration of 100 μM, and the protein was placed at 4 °C overnight to allow complete incorporation of vanadate into the active site of the protein. Excess salt was removed by dialysis (SpectraPor membrane, 25 kDa molecular weight cutoff) against 25 mM Tris acetate, pH 8.3, containing 100 μM sodium orthovanadate. The final dialysis step was conducted against solution containing 25 mM Tris acetate, pH 8.3 to remove any sodium and excess vanadate. The final sample conditions were similar to those at which the X-ray structure determination was carried out.

The protein was concentrated using Amicon Centricon-Plus 30 (30 000 molecular weight cutoff) filter devices. The purified protein solution was stored at -80 °C until further analysis. Characterization of the protein was done using SDS-PAGE, and quantification was carried out by Bradford assay. Protein yield was approximately 80 mg per 1 L of cell culture. Throughout the purification procedure, enzyme activity was monitored qualitatively by the phenol red assay and

quantitatively by the MCD assay.⁷ The specific activity of the purified, concentrated protein was approximately 16 units/mg, in excellent agreement with the previous reports.³⁸ The vanadate incorporation, calculated by measuring the activity using MCD assay with and without vanadate, was found to be approximately 98%.

Preparation of VCPO Sample for ⁵¹V Solid-State NMR Spectroscopy. The concentrated protein was lyophilized using a vacuum centrifuge, and 68 mg of the lyophilized protein were packed into a 5 mm Doty SiN₃ thick-wall rotor. The packed rotor was then stored at -20 °C until required for the solid-state NMR experiments.

Enzymatic activity was assessed before and after the NMR experiments. The activity remained intact according to the assay conducted on small portions of the lyophilized VCPO sample employed in the SSNMR experiments.

⁵¹V Solid-State NMR Spectroscopy of Vanadium Chloroperoxidase. ⁵¹V solid-state NMR spectra were acquired at 157.64539 MHz (14.1 T) on a Varian InfinityPlus narrow-bore spectrometer using a 5 mm Doty XC5 single-channel MAS probe, at spinning frequencies of 15 and 17 kHz. The spinning frequency was controlled to within ±2 Hz. The temperature was maintained between -25 and -26 °C throughout the measurements, according to the readings on the temperature controller. The actual sample temperature is spinning frequency-dependent and is higher by 12° and 15° for 15 and 17 kHz, respectively. The magic angle was adjusted using NaNO₃ (by detecting the ²³Na MAS signal). The radio frequency field strength was 44.6 kHz (nonselective 90-degree pulse of 5.6 μs), as calibrated using the ⁵¹V signal from the neat VOCl₃ liquid. A single 1.45-μs pulse (a 23° flip angle) was employed to excite the central and the satellite transitions; 0.3-s recycle delays were used. The spectral widths were 1 MHz, and 4096 complex data points were acquired for each FID. A total of 1.6 million or 1.5 million transients were added in the final spectra acquired with the spinning frequencies of 15 kHz and 17 kHz, respectively. Nutation spectra³⁹ were acquired with 50 000 transients for each t₁ point; a total of 11 points were acquired with the excitation pulse length varied between 1.45 and 11.5 μs.

Data were processed by left shifting the spectrum to the first rotor echo to suppress baseline distortions, followed by exponential apodization, with linebroadening of 500 Hz. Isotropic chemical shifts were reported with respect to the external reference, neat VOCl₃.

⁵¹V Solid-State NMR Spectroscopy of Model Oxovanadium(V) Complexes. ⁵¹V solid-state NMR spectra of model oxovanadium(V) complexes were acquired at 105.2 MHz (9.4 T) on a Tecmag Discovery spectrometer using a 4 mm Doty XC4 MAS probe. Spectra were recorded using 5–40 mg of sample. For each of the compounds, spectra at three different spinning speeds ranging between 10 and 17 kHz were acquired. The spinning speed was controlled to within ±2 Hz. The magic angle was adjusted using NaNO₃ (by detecting the ²³Na MAS signal). A single 1-μs pulse ($\gamma H_1/2\pi \approx 80$ kHz) was employed to excite the central and the satellite transitions; 0.5-s recycle delays were used. The spectral widths were 1.25 MHz. 4096 complex data points were acquired. The data were processed by linear prediction of the first 66 points to suppress baseline distortions, followed by Fourier transformation and baseline correction. Isotropic chemical shifts are reported with respect to neat VOCl₃, whose ⁵¹V spectrum was recorded and used as an external referencing standard.

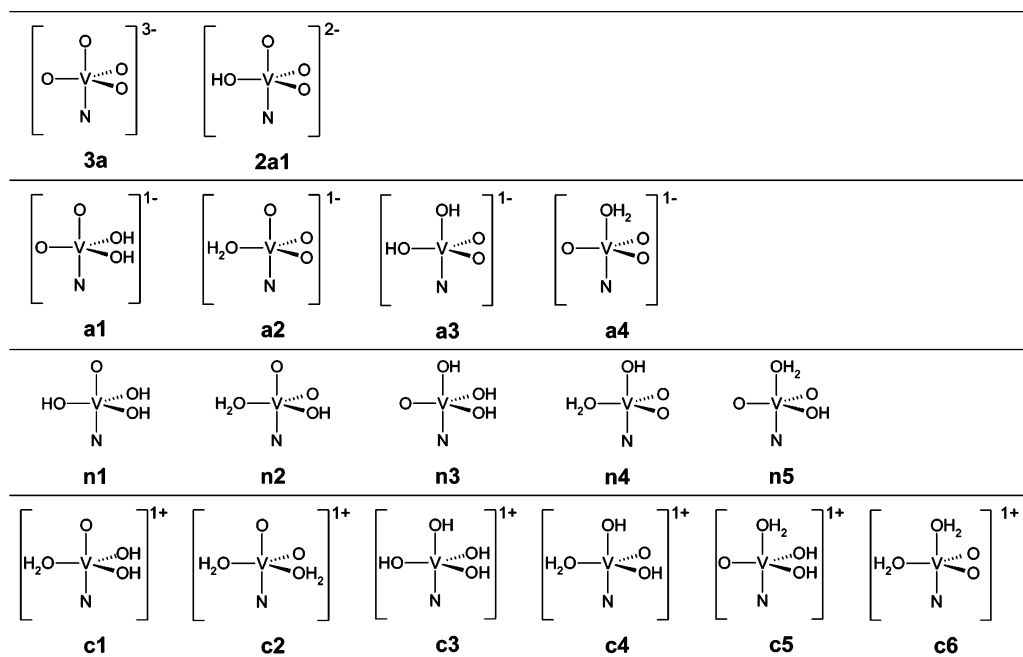
Numerical Simulations of the NMR Spectra. Numerical simulations of the experimental ⁵¹V solid-state NMR single-pulse and nutation spectra of the protein, acquired at 15 and 17 kHz, were performed using SIMPSON,²⁸ under a Linux environment. The combined effect of the quadrupolar interaction to second-order and chemical-shift anisotropy was taken into account in the simulations. Nutation curves were analyzed in IgorPro (Wavemetrics, Inc.), and the least-squares analysis of the experimental and simulated curves was performed using a home written program in Mathematica (Wolfram, Inc.). The seven indepen-

(36) Bryce, D. L.; Wasylishen, R. E. *Phys. Chem. Chem. Phys.* **2002**, *4* (15), 3591–3600.

(37) Ooms, K. J.; Wasylishen, R. E. *J. Am. Chem. Soc.* **2004**, *126* (35), 10972–10980.

(38) Hemrika, W.; Renirie, R.; Macedo-Ribeiro, S.; Messerschmidt, A.; Wever, R. *J. Biol. Chem.* **1999**, *274* (34), 23820–23827.

(39) Samoson, A.; Lippmaa, E. *J. Magn. Reson.* **1988**, *79* (2), 255–268.

Chart 1. Schematic Representations of the Smallest Size VCPO Active Site Models Used in the DFT Calculations of the NMR Spectroscopic Observables

dent parameters describing the quadrupolar and CSA tensor anisotropies (C_Q , η_Q , δ_σ , and η_σ) and the relative tensor orientations (the Euler angles α , β , and γ) were obtained by the least-squares fitting of the simulated and experimental sideband intensities using a program written in our laboratory under the Mathematica (Wolfram, Inc.) environment. The quadrupolar and CSA tensor elements are defined in a spherical harmonics basis set as described in the previous section (eqs 5 and 6).

Quantum Mechanical Calculations of Electric Field Gradient and Magnetic Shielding Anisotropy Tensors. The density functional theory calculations of electric field gradient and nuclear magnetic shielding tensors were performed under Gaussian03.⁴⁰

Becke's three-parameter hybrid B3LYP functional was used for all calculations.⁴¹ The calculations were conducted with three different basis sets for small VCPO active site models. The TZV basis set⁴² and effective core potentials for vanadium atoms were used for one set of the calculations; in another set the 6-311+G basis set was employed. Full geometry optimizations were performed for the fifteen smallest models and compounds resulting in the energetically most stable structures, using the starting coordinates utilized by Carlson, Pecoraro, De Gioia, and colleagues and the same basis set utilized in their work.¹⁴ For the V atom, the effective core potential basis set LanL2DZ^{43–46} was modified to replace the two outermost p functions by a (41) split of the optimized 4p function (341/341/41).⁴⁷ For N and O atoms, the cc-pVDZ⁴⁸ basis set was employed, and for H, D95.⁴³ In all cases, the structures converged to the same geometries as reported in the above work. Therefore, for the remaining models the minimized structures obtained by these authors were employed without further geometry optimization for calculations of the NMR parameters.

The nuclear magnetic shielding calculations were performed using the gauge-including atomic orbitals (GIAO) method,^{49,50} as implemented

in Gaussian03. The isotropic chemical shifts are calculated with respect to VOCl_3 optimized at the same level of theory. The computed absolute shieldings for VOCl_3 were -2317.24 and -2279.39 ppm for the TZV and 6-311+G basis sets, respectively. We note that, for completeness, we report the computed isotropic chemical shifts in the Supporting Information but do not use them in the data analysis as they rely on the accuracy of the minimized structure for the reference compound, VOCl_3 . We focus instead solely on the tensorial anisotropic parameters C_Q , η_Q , δ_σ , and η_σ .

A set of 86 active site models of VCPO were addressed. These were examined earlier by Carlson, Pecoraro, De Gioia, and colleagues, who investigated their energetic and structural parameters to determine the most likely resting state coordination environment of VCPO.¹⁴ The nomenclature used in this work follows Carlson, Pecoraro, De Gioia, and colleagues.¹⁴ Specifically, the first part of the name corresponds to the charge of the vanadate cluster: **a**, **n**, or **c** to describe the anionic, neutral, or cationic species, respectively. A preceding number refers to the charge of the system if different from one or zero (e.g., **2c** for the +2 charge). The number following the letter corresponds to the starting structure of the vanadate unit defined in Chart 1. If a superscript follows, it will designate each external hydrogen-bonding molecule present in the structure. K, n, or c refers to a potassium ion, a neutral hydrogen-bond donor, or positively charged hydrogen-bonding molecule, respectively. If a particular species was reported to contain more than one local energy minimum it will additionally contain the subscript **i**, **ii**, **iii**, or **iv**, depending on the number of minima observed. The bound ligand (imidazole or ammonia) mimicking His-496 is designated as N. In Chart 1, the schematic representations of the smallest size models are shown.

Results

⁵¹V NMR Spectra of Vanadium Chloroperoxidase. In Figure 2, ⁵¹V magic angle spinning NMR spectra are demonstrated for vanadium chloroperoxidase acquired with spinning frequencies of 15 and 17 kHz.

(40) Frisch, M. J. et al. *Gaussian 98*, revision A.1x; Gaussian, Inc.: Pittsburgh, PA, 2001.

(41) Becke, A. D. *J. Chem. Phys.* **1993**, *98* (7), 5648–5652.

(42) Schafer, A.; Huber, C.; Ahlrichs, R. *J. Chem. Phys.* **1994**, *100* (8), 5829–5835.

(43) Dunning, T. H. J.; Hay, P. J. In *Modern Theoretical Chemistry*; Schafer, H. F. I., Ed.; Plenum Press: New York, 1976; Vol. 3, pp 1–28.

(44) Hay, P. J.; Wadt, W. R. *J. Chem. Phys.* **1985**, *82* (1), 270–283.

(45) Hay, P. J.; Wadt, W. R. *J. Chem. Phys.* **1985**, *82* (1), 299–310.

(46) Wadt, W. R.; Hay, P. J. *J. Chem. Phys.* **1985**, *82* (1), 284–298.

(47) Couty, M.; Hall, M. B. *J. Comput. Chem.* **1996**, *17* (11), 1359–1370.

(48) Woon, D. E.; Dunning, T. H. *J. Chem. Phys.* **1993**, *98* (2), 1358–1371.

(49) Ditchfield, R. *Mol. Phys.* **1974**, *27* (4), 789–807.

(50) Wolinski, K.; Hinton, J. F.; Pulay, P. *J. Am. Chem. Soc.* **1990**, *112* (23), 8251–8260.

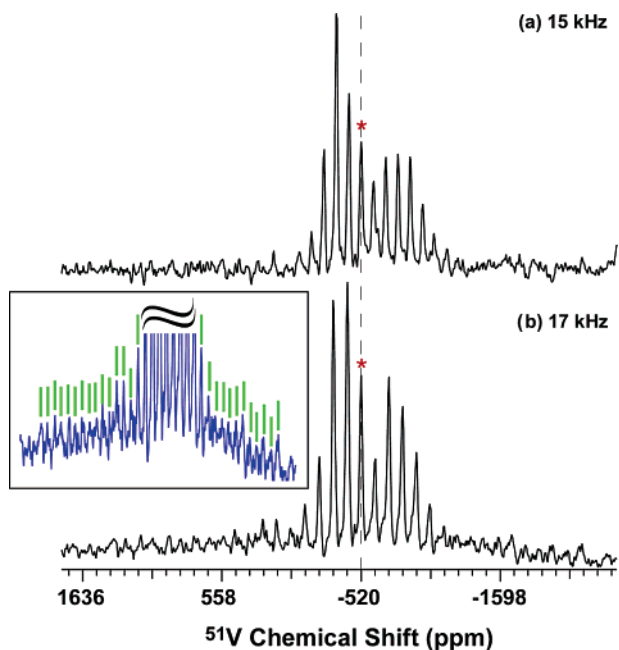


Figure 2. ^{51}V magic angle spinning NMR spectra of vanadium chloroperoxidase acquired at 14.1 T with the MAS spinning frequencies of (a) 15 kHz and (b) 17 kHz. The observed isotropic chemical shift (-520 ppm, not corrected for the quadrupole-induced shift) is labeled with an asterisk in each of the spectra. The inset is a vertical expansion of the 17 kHz spectra to illustrate that (weak) satellite transition spinning sidebands (guided with green markers) extend to the entire spectral range, indicating a large quadrupolar coupling constant.

The shape of the spinning sideband (ssb) manifold indicates large chemical shift anisotropy resulting in the asymmetric central transition. The central transition sidebands dominate the overall spectrum. However, careful examination of the 17 kHz spectrum reveals that weak spinning sidebands corresponding to the satellite transition span the entire spectral range (illustrated in the inset to Figure 2). This is an indication of a large quadrupolar anisotropy. More convincing evidence for a large C_Q is presented below. Qualitative analysis of the ^{51}V MAS (17 kHz) spectrum of the model bioinorganic complex benzhydroxamato- $\{N$ -(2-oxiphenyl)-5,6-dibenzosalicylideneaminato}-oxovanadium(V) (Figure 3c) and of 9.4 T spectra of model oxovanadium(V) complexes reported by us earlier¹⁹ suggests that the quadrupolar coupling constant in the spectra of VCPO is considerably larger than that in the $\text{VO}_2(\text{acpy-inh})$ complex exhibiting the largest C_Q of 7 MHz in the series. However, due to the large magnitude of quadrupolar anisotropy and the limited signal-to-noise ratio, the single-pulse spectra alone are not sufficient for extracting the precise value of C_Q . As will be described in the subsequent sections, analysis of the central transition line shapes also was necessary, and the combination of these two measurements yielded the desired parameter.

The total acquisition time for the spectra presented in Figure 2 was 5.2 and 5.5 days, to achieve the highest practically attainable signal-to-noise ratio. However, spectra of a signal-to-noise ratio adequate for subsequent numerical simulations have been collected within 20.8 h (Figure 3d), suggesting that detection of the long-lived intermediate species of vanadium haloperoxidases might be feasible at low temperatures. Furthermore, based on our experience with the magnetic field dependence of the ^{13}C multidimensional NMR spectra of proteins⁵¹ we anticipate a gain in sensitivity close to a factor of

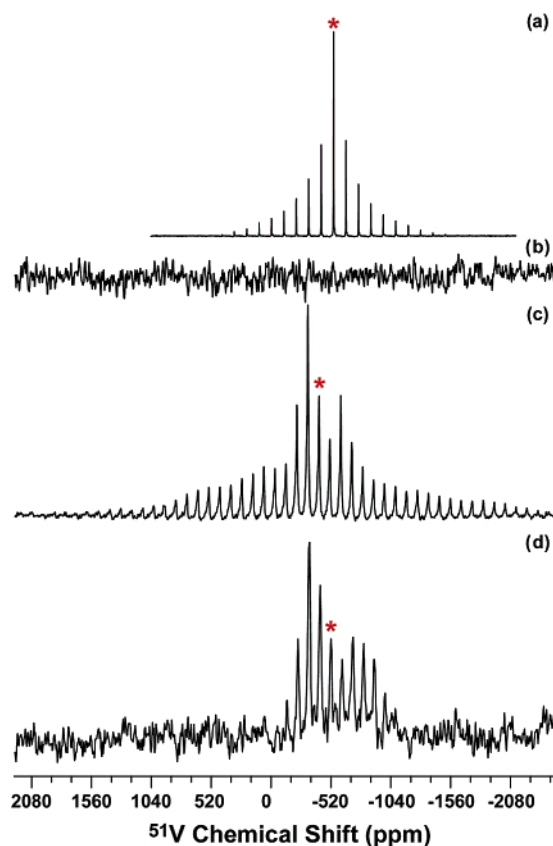


Figure 3. 14.1 T ^{51}V NMR spectra of (a) Na_3VO_4 ; (b) bovine serum albumin (BSA), prepared as described in the Experimental Section, (c) benzhydroxamato- $\{N$ -(2-oxiphenyl)-5,6-dibenzosalicylideneaminato}-oxovanadium(V), and (d) vanadium chloroperoxidase. Spectra (b) and (d) were collected with 250 000 scans under identical experimental conditions, processed with exponential apodization and line broadening of 1 kHz. The isotropic peaks are indicated by an asterisk, where applicable.

2 at fields of 17.6 T. We also note that it would be desirable to conduct the ^{51}V solid-state NMR experiments with hydrated proteins prepared by controlled precipitation from poly(ethylene glycol); this procedure typically results in conformationally homogeneous samples and narrow lines.^{51,52} However, in this first set of measurements testing the feasibility of ^{51}V SSNMR in a protein we needed to ensure that the maximum possible amount of sample could be placed in the rotor. Therefore, VCPO was prepared in lyophilized form.

Generally, we expect that conducting these experiments at higher magnetic fields and higher MAS spinning frequencies will permit minimizing the amount of protein sample and/or experiment time thus expanding the range of vanadium proteins amenable to studies by ^{51}V MAS NMR spectroscopy.

Verification of ^{51}V NMR Signal from the Protein. A number of control experiments were conducted in order to unambiguously assign the observed signal to the vanadate bound in the active site of the protein. In Figure 3, the ^{51}V spectra shown were acquired for the following samples, to eliminate the possibility that the signal might be arising from the unbound vanadate species: (a) Na_3VO_4 , (b) bovine serum albumin (BSA) (200 mg/mL in 25 mM tris acetate buffer, pH 8.3) incubated overnight in a final concentration of 100 μM Na_3VO_4 , followed

(51) Marulanda, D.; Tasayco, M. L.; Cataldi, M.; Arriaran, V.; Polenova, T. *J. Phys. Chem. B* **2005**, *109* (38), 18135–18145.

(52) Marulanda, D.; Tasayco, M. L.; McDermott, A.; Cataldi, M.; Arriaran, V.; Polenova, T. *J. Am. Chem. Soc.* **2004**, *126* (50), 16608–16620.

by dialysis and lyophilization in the same manner as that described for the VCPO, (c) model compound benzhydroxamato- $\{N$ -(2-oxiphenyl)-5,6-dibenzosalicylideneaminato}-oxovanadium(V), and (d) vanadium chloroperoxidase.

The spectrum of Na_3VO_4 illustrating the unbound vanadate species does not exhibit any significant chemical shift anisotropy, and the isotropic chemical shift of -544 ppm does not correspond to any of the sidebands identified in the protein spectra. As expected, BSA does not produce any detectable signal, suggesting that any free or nonspecifically bound vanadate would be removed during the dialysis step of purification. On the other hand, the spectra of the model bioinorganic compound benzhydroxamato- $\{N$ -(2-oxiphenyl)-5,6-dibenzosalicylideneaminato}-oxovanadium(V) exhibit an asymmetric lineshape characteristic of a large chemical shift anisotropy, in agreement with the 9.4 T spectra reported previously for this compound.¹⁹ Furthermore, the spinning sideband envelope spans over 4000 ppm, and the relative spinning sideband intensities of the satellite transitions are stronger than those in the corresponding VCPO spectrum (Figure 2b). As the quadrupolar coupling constant for this compound is 3.9 MHz,¹⁹ we conclude that the quadrupolar interaction in the protein must be much stronger. Additionally, the broader central transition in VCPO indicates that the chemical shift anisotropy is more substantial than that in the model complex, as described in more detail below.

Numerical Simulations of ^{51}V Spectra. The difference of many orders of magnitude in the quadrupolar and chemical shift anisotropies ($H_Q^{(1)} > H_{\text{CSA}} > H_Q^{(2)}$) ensures efficient separation of variables corresponding to these two interactions. As was demonstrated by several previous reports from our and other laboratories,^{18,19,22,23,31,32,35} the seven parameters describing the two tensors and their mutual orientations can be readily extracted by numerical simulations of the full spinning sideband manifold.

In the case of vanadium chloroperoxidase, the large size of the quadrupolar interaction results in relatively weak spinning sideband intensities spread over the entire spectral range, and with the currently attainable sensitivity of the experiments, determination of the exact value of the C_Q from the single pulse spectra alone is not feasible. On the other hand, due to the natural separation of variables in the spectra, the CSA tensor elements can be readily determined from simulating the spinning sideband envelope of the central transition. Numerical SIMPSON simulations for both MAS spinning frequencies (15 and 17 kHz) yield excellent agreement of the CSA parameters, and the best fit values are $\delta_\sigma = -520 \pm 13$ ppm and $\eta_\sigma = 0.4 \pm 0.05$. In Figure 4, the experimental and best-fit simulated spectra are demonstrated for the MAS frequency of 17 kHz. The inset displaying an overlaid experimental and simulated spectrum illustrates the high quality of the fit. It is also worth noting that good agreement between the experimental and the simulated central transition spectra is achieved regardless of the quadrupolar coupling constant used in the simulation, in the ranges $C_Q < 1$ and $4 \text{ MHz} < C_Q < 13 \text{ MHz}$, attesting to the independence of the spectral parameters corresponding to quadrupolar and the CSA interactions. As described below, when $C_Q > 13 \text{ MHz}$, the second-order linebroadening is much larger than that in the experimental spectra. When $1 \text{ MHz} < C_Q < 4 \text{ MHz}$, the intensities of the satellite-transition spinning sidebands are comparable in magnitude with those of the central

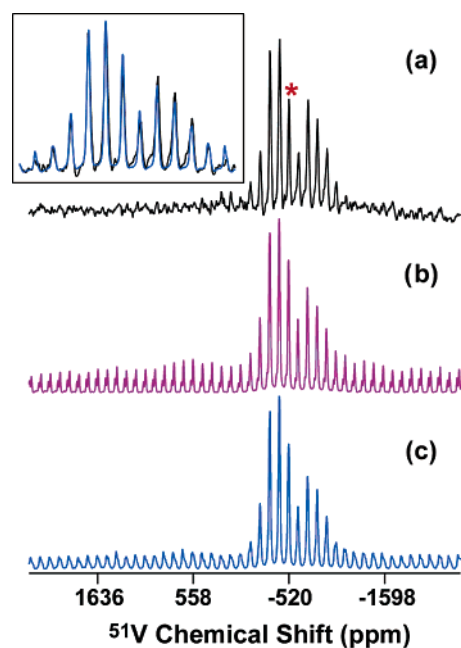


Figure 4. ^{51}V MAS (17 kHz) NMR spectra of vanadium chloroperoxidase: (a) experimental and (b and c) simulated in SIMPSON using the best fit parameters: $C_Q = 10.5 \text{ MHz}$, $\eta_Q = 0.55$, $\delta_\sigma = -520 \text{ ppm}$, $\eta_\sigma = 0.4$. The isotropic shift corrected for the second-order quadrupolar-induced shift is -507.5 ppm . In the simulated spectrum (c), the magic angle mis-set by 0.2° was taken into account. The inset is an overlay of the experimental and simulated central transition spinning sidebands, to demonstrate the quality of the fit.

transition, which is not in any agreement with the experimental data. Furthermore, the experimental ^{51}V MAS spectra of the model compound benzhydroxamato- $\{N$ -(2-oxiphenyl)-5,6-dibenzosalicylideneaminato}-oxovanadium(V) with $C_Q = 3.9 \text{ MHz}$ ¹⁹ (Figure 3c) exhibit very strong satellite transition sidebands. We therefore conclude that the quadrupolar coupling constant in VCPO must be significantly larger than 4 MHz.

The values of C_Q and η_Q can in principle be deduced from nutation spectra.³⁹ Toward that end a nutation curve consisting of 11 points was obtained by signal averaging over a two day period, and the result (not shown here) was compared with a series of theoretical spectra calculated with SIMPSON. Unfortunately, the poor signal-to-noise ratio did not allow a meaningful analysis of the data. The experimental and calculated nutation profiles are documented in the Supporting Information.

To estimate C_Q , we have performed the analysis of lineshapes and linewidths of the individual spinning sidebands of the central transition. Figure 5 illustrates the ssb linewidths as a function of C_Q . Expansions of the overlaid experimental and simulated spectra shown on the right demonstrate that good agreement between these is only reached when C_Q is in the range between 9 and 13 MHz. However, it is conceivable that an inhomogeneous distribution of the isotropic shift due to possible conformational heterogeneity in the protein sample is present. This may introduce additional linebroadening to the experimental spectra, resulting in an overestimated C_Q .

To assess the contribution of the inhomogeneous line broadening to the total linewidths, we examined the lineshapes in the spectra of the following model compounds, addressed in our recent work: benzhydroxamato- $\{N$ -(2-oxiphenyl)-5,6-dibenzosalicylideneaminato}-oxovanadium(V) (SJZ0032), 3-oxiflavone- $\{3$ -methoxisalicylidene- α -(oxibenzylidenehydrazonato)-

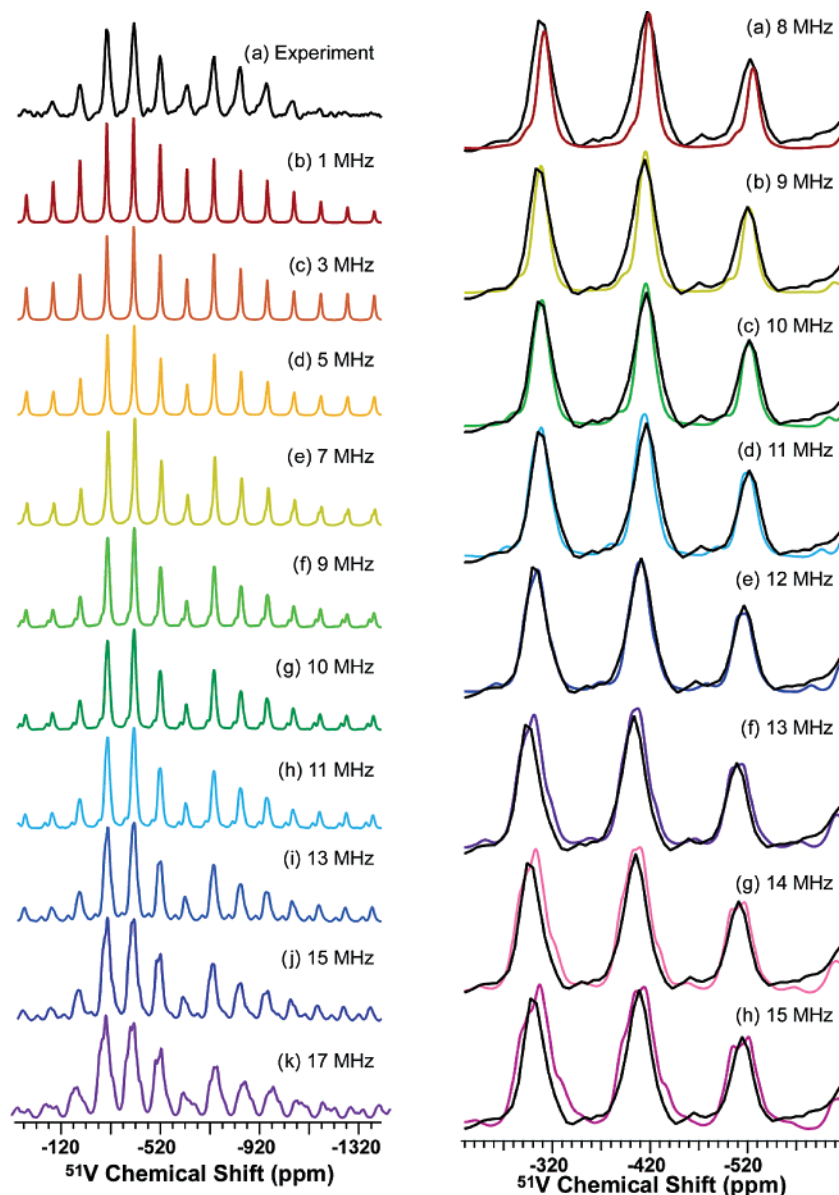


Figure 5. Spinning sideband envelope profiles (left) and sideband lineshapes (right) of the central transition in ^{51}V 17 kHz MAS spectra for different values of C_Q . On the left, (a) is the experimental VCPO spectrum, while (b)–(k) are simulated spectra for the C_Q values in the range 1–17 MHz. On the right, expansions of the experimental spectrum are overlaid with the simulated spectra for C_Q of 8–15 MHz to illustrate the range of possible experimental C_Q 's. Experimental and simulated FIDs were multiplied by an exponential function (linebroadening of 1.5 kHz) prior to the Fourier transformation. Note that reasonable agreement between the experimental and simulated lineshapes is reached when C_Q is in the range 9–13 MHz.

oxovanadium(V) (SJZ0060), benzhydroxamato-(3-methoxy- α -hydroxybenzylidenehydrazonato)-oxovanadium(V) (SJZ0068), (oxo)bis[oxobis(8-quinolinolato) vanadium(V)] (HS001), ammonium oxoperoxo(pyridine-2,6-dicarboxylato)vanadate(V) hydrate (HS003), salicylaldehyde-[(benzylmercapto)-thiocarbonyl]-hydrazone (Sal5OEt), and acetylpyridine-(isonicotinic acid hydrazide)-dioxovanadium(V) ($[\text{VO}_2(\text{acpy-inh})]$).¹⁹ For these complexes, the quadrupolar and chemical shift tensor elements have been previously determined, and C_Q values range between 3.65 and 7.00 MHz.¹⁹ Furthermore, SJZ0032 is an amorphous compound, while the remaining six complexes are polycrystalline.

In Figure 6, the experimental (9.4 T) and simulated (9.4 and 14.1 T) lineshapes are illustrated for the six polycrystalline compounds SJZ0060, SJZ0068, HS001, HS003, Sal5OEt, and $[\text{VO}_2(\text{acpy-inh})]$. The simulated and experimental lines are in very good agreement, indicating that when oxovanadium (V)

solids exhibit long-range order and inhomogeneous linebroadening is consequently not anticipated, the observed and simulated lineshapes are in close agreement.

In Figure 7, the experimental and simulated lineshapes are demonstrated for the amorphous model complex SJZ0032, at two different field strengths: 14.1 and 9.4 T. In contrast to the polycrystalline compounds, the experimental spectra for this complex have broader lines than expected based on its C_Q of 3.9 MHz, due to the inhomogeneous linebroadening and perhaps to the presence of additional species. The experimental linewidths at half-maximum are 1.15 kHz (10.9 and 7.7 ppm at 9.4 and 14.1 T, respectively), while the expected linewidths for a C_Q of 3.9 MHz and $\eta_Q = 0.77$ are 0.9 and 0.7 kHz (7.7 and 4.4 ppm), respectively. Therefore, the inhomogeneous line broadening is estimated to be ca. 3.2–3.3 ppm and, as expected, is magnetic-field-independent. The extra broadenings in the lower portions of the peaks are about 25 and 9 ppm, respectively.

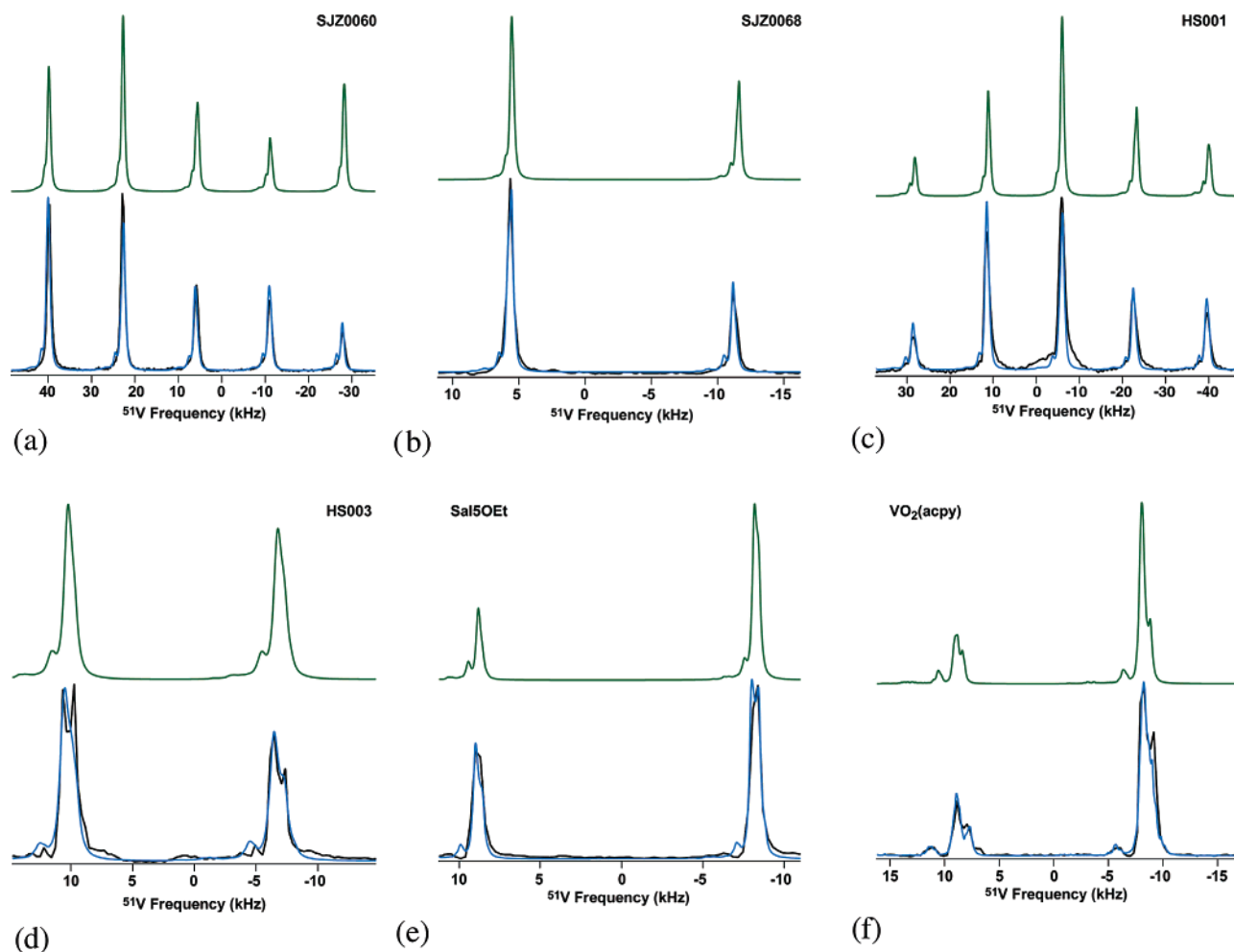


Figure 6. Experimental and simulated lineshapes of the central transition spinning sidebands for polycrystalline model oxovanadium(V) solids: (a) SJZ0060 ($C_Q = 5.10$ MHz, $\eta_Q = 0.60$), (b) SJZ0068 ($C_Q = 3.65$ MHz, $\eta_Q = 0.22$), (c) HS001 ($C_Q = 5.67$ MHz, $\eta_Q = 0.45$), (d) HS003 ($C_Q = 6.23$ MHz, $\eta_Q = 0.20$), (e) Sal5OEt ($C_Q = 4.35$ MHz, $\eta_Q = 0.00$), and (f) [VO₂(acpy-inh)] ($C_Q = 7.00$ MHz, $\eta_Q = 0.25$). For each compound, the bottom spectra represent the experimental (black) and the simulated (blue) spectra at 9.4 T. The top spectrum (green) is a simulated spectrum at 14.1 T (experimental data are not available).

Table 1. Calculated ⁵¹V Linewidths for the Isotropic Spinning Sideband for Different Values of C_Q

C_Q , MHz	linewidth, ppm
8	13.6
9	16.2
10	18.1
11	21.6
12	24
13	27.6
14	32.4
15	36.6

The discrepancy between these two numbers indicates that this broadening does not originate in isotropic shift broadening. We believe that this broadening is due to the effect of magic-angle mis-setting on the satellite sidebands, as discussed below.

Comparison of the structures of model complexes and VCPO active site strongly suggests that the inhomogeneous linebroadening in VCPO does not exceed that of SJZ0032. The experimental linewidth in the protein spectra is 24 ppm. Taking into account the possible inhomogeneous linebroadening, we estimate the homogeneous linewidth to be ca. 20–21 ppm. This corresponds to a C_Q value of 11 MHz (Table 1), and even if we allow for an inhomogeneity broadening between 0 and 8 ppm, we can entirely rule out C_Q below 9 or above 13 MHz.

Based on the above independent pieces of information we conclude that $C_Q = 10.5 \pm 1.5$ MHz, and $\eta_Q = 0.55 \pm 0.15$.

With these quadrupolar anisotropy tensor parameters, we repeated the calculations of the single pulse spectra. The best fits of the ssb intensities were obtained with $\eta_Q = 0.65$ (Figure 4). However, reasonable agreement with the experimental data is reached for the range of η_Q values between 0.4 and 0.9.

It is also worth noting that the spinning sideband intensities of the outer satellite transitions in the experimental spectrum are weaker than expected for a C_Q of 10.5 MHz. We attribute this to the inevitable errors in the magic angle settings arising because of long experiment times and high MAS frequencies. In fact, these errors are readily estimated by numerical simulations in SIMPSON, and in our case range between 0.1° and 0.2°. In Figure 4c simulated spectra with the magic angle mis-set by 0.2° illustrate the attenuated satellite transition spinning sideband intensities.

Density Functional Theory Calculations of NMR Spectroscopic Observables. To understand the structural and electronic properties of the vanadium center giving rise to the experimental NMR observables, we computed the NMR parameters for an extensive series of 86 VCPO active site models, using density functional theory. These complexes are related

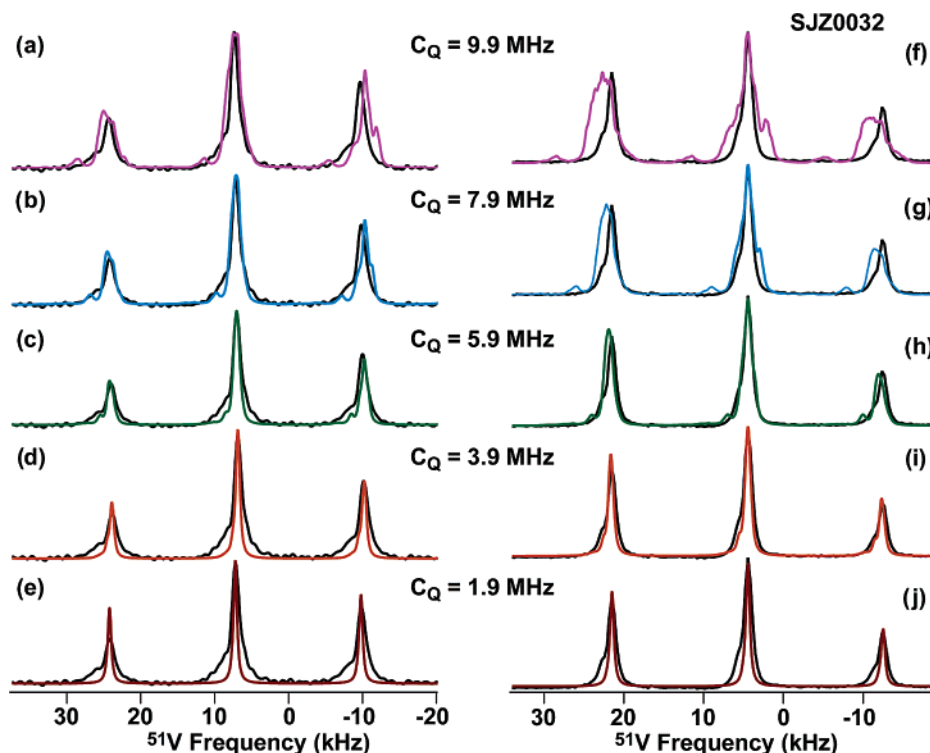


Figure 7. Experimental (black) and simulated (colored) lineshapes of the central transition spinning sidebands for amorphous model oxovanadium(V) compound SJZ0032 ($C_Q = 3.90$ MHz, $\eta_Q = 0.77$). The left set of spectra (a–e) are for the magnetic field of 14.1 T, and the right set (spectra f–j), for 9.4 T. The spectra were simulated assuming different values of C_Q ranging between 1.9 and 9.9 MHz as specified in the figure. The apparent linewidth is larger than that expected for a C_Q of 3.9 MHz due to the inhomogeneous linebroadening.

to the resting state of VCPO and model the different possible coordination environments and protonation states of the vanadium center in the protein. As was already mentioned, these models were addressed previously by Carlson, Pecoraro, De Gioia, and colleagues, who investigated their energetic and structural parameters to determine the most likely coordination environment of the resting state of VCPO.¹⁴

We employed two different extended basis sets TZV and 6-311+G in calculations of the NMR spectroscopic observables. The results of the calculations with both sets are generally in good agreement, as we have previously observed for bioinorganic oxovanadium(V) complexes.¹⁹ The complete summary of the calculations for all models is presented in Table 1s of the Supporting Information.

In Table 2, the computed NMR parameters are presented for the smallest structures (**2a1**, **2akk**, **a1-a4**, **n1-n5**, and **c1-c6**), for the complexes where calculated observables agree with experimental results (**a3ⁿ_{i-ii}**, **a3ⁿⁿ**, **a3^{ncc}**, **a3^{nncc}**, **c5ⁿ_{i-ii}**, **c6ⁿ_{i-ii}**, **n2ⁿ_{iii-v}**), and for models proposed to be the plausible resting state structures based on their low energies (**n3^c_{i-ii}**, **n3ⁿ_{i-vii}**, **n3ⁿⁿ**, **n5^c_{i-ii}**, **n5ⁿ_{i-iii}**, **n5^{nc}**, **n5ⁿⁿ_{ii}**). We consider that calculations are in reasonable agreement with experiment only when the magnitudes of both quadrupolar and CSA tensors (C_Q and δ_σ) are within 15–20% of the experimentally determined values.

Remarkably, only a very limited set of models yield computed NMR parameters in agreement with the experimental NMR results: **a3**, **a3ⁿ_{i-ii}**, **a3ⁿⁿ**, **a3^{ncc}**, **a3^{nncc}**, **c5ⁿ_{i-ii}**, **c6ⁿ_{i-ii}**, **n2ⁿ_{iii-v}**. Furthermore, the majority (seven) of these represent an anionic vanadate cofactor with an axial hydroxo ligand, one hydroxo-, and two oxo- groups in the equatorial plane (the parent structure **a3**). This set of complexes with the parent **a3** structure was also identified by Carlson, Pecoraro, De Gioia, and colleagues

as the most likely resting state configuration of the vanadate cofactor representing the lowest energy structures in the DFT calculations of active site complexes as well as in the QM/MM calculations of a large VCPO model.^{14,17}

Interestingly, the identity of the hydrogen bonding partners or inclusion of extended models of the active-site residues had a relatively minor impact on the quadrupolar coupling constant, which varied between 9.2 and 12.8 MHz. Note that the experimentally determined C_Q spans essentially the same range (10.5 ± 1.5 MHz) as the theoretically predicted constants. On the other hand, the asymmetry parameter of the quadrupolar tensor, η_Q , was sensitive to the specific environment of the parent anionic vanadate and varied from 0.08 in **a3ⁿⁿ** to 0.89 in **a3^{nncc}**. The most extended models **a3^{nncc}** and **a3^{nncc}** displayed the largest η_Q values. The experimental results suggest $\eta_Q = 0.55 \pm 0.15$, and the calculations for the extended models are in reasonable agreement with the experiment. The Euler angles α , β , and γ describing the relative orientations of the quadrupolar and CSA tensors also displayed significant variations in the presence of additional ligands. With one exception (**a3^{ncc}**), the calculations predicted a negative sign for the quadrupolar coupling constant. However, only the magnitude of C_Q is determined in the NMR experiments, and therefore we cannot rule out any of the models based on the computed sign of the quadrupolar coupling constant. The experimental and computational results indicate that the current precision of the experimentally determined quadrupolar tensor is such that we cannot yet probe the nature of the ligands beyond the first coordination sphere. Higher sensitivity will be required to overcome the current limitations.

Somewhat surprisingly, we found that three complexes with the overall neutral vanadate cofactor **n2ⁿ_{iii-v}** yielded computed

Table 2. Calculated NMR Parameters for Vanadium Complexes – VCPO Active Site Models^a

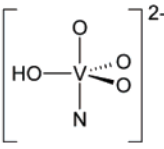
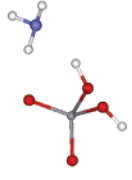
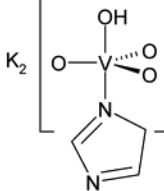
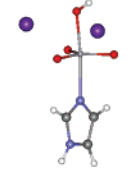
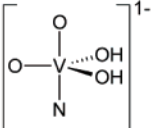
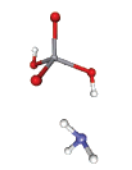
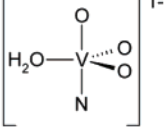
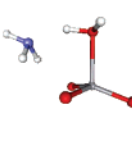
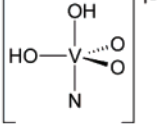

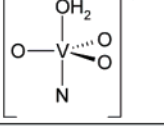
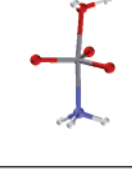
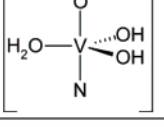
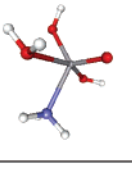
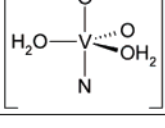
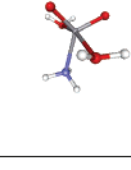
		C_q (MHz)	η_q	δ_σ (ppm)	η_σ	Euler angles		
						α	β	γ
Basic structures								
2a1 		4.31	0.477	-263.289	0.0982	-24.4	4.20	49.8
2akk 		-18.8 -21.1	0.264 0.293	429.768 442.254	0.131 0.129	-2.73 -2.16	1.60 1.75	2.12 1.50
a1 		4.31 5.77	0.477 0.456	-263.289 -261.654	0.0982 0.0950	-24.4 -24.3	4.20 4.20	49.8 50.4
a2 		-18.6 -21.2	0.134 0.146	-129.980 -132.787	0.0131 0.0277	60.6 15.0	0.736 0.703	-48.0 -11.5
a3 		-9.72 -11.3	0.352 0.438	-572.892 -568.340	0.135 0.144	3.40 2.58	1.84 1.89	-47.7 -47.5
a4 		-17.5 -20.0	0.124 0.137	-161.580 -163.383	0.0646 0.0886	14.8 23.8	0.00179 0.00169	-37.4 -58.1
c1 		-5.97 -7.04	0.483 0.309	-440.446 -430.348	0.247 0.253	84.3 82.6	12.4 12.1	-32.6 -33.9
c2 		-14.0 -16.4	0.391 0.513	-736.727 -739.405	0.197 0.147	90.0 -90.0	2.45 2.46	-90.0 89.9

Table 2 (Continued)

		C_Q (MHz)	η_Q	δ_σ (ppm)	η_σ	Euler angles		
						α	β	γ
Basic structures								
c3		3.45 3.99	0.990 0.989	401.289 404.214	0.163 0.166	47.3 45.2	10.3 10.2	79.1 78.4
c4		-7.06 -8.20	0.164 0.257	-489.605 -480.613	0.177 0.179	23.3 23.0	5.58 5.69	-75.6 -76.5
c5		-11.6 -13.7	0.916 0.748	-647.871 -638.367	0.150 0.191	85.3 85.3	15.6 15.3	86.1 85.9
c6		9.59 12.0	0.978 0.872	-626.602 -628.727	0.338 0.312	-81.7 -82.3	0.00726 0.00744	80.4 81.0
n1		-2.27 2.34	0.636 0.991	-207.775 -202.296	0.0485 0.0458	-1.21 -1.26	2.56 2.89	0.0338 0.166
n2		-11.5 -13.5	0.323 0.386	-310.922 -305.505	0.206 0.198	-21.1 -21.3	2.90 2.97	65.0 66.5
n3		-5.03 -6.03	0.659 0.541	-454.623 -449.705	0.216 0.226	69.1 68.7	6.18 6.07	-25.8 -27.6
n5		-17.5 -20.1	0.105 0.0332	-596.336 -596.146	0.128 0.156	-82.9 -81.1	3.94 3.93	89.4 89.9
Extended structures								
a3ni_oxide		-9.20 -10.8	0.238 0.319	-539.316 -535.455	0.152 0.165	63.7 65.2	2.91 2.89	-17.0 -17.3

Table 2 (Continued)

		C_Q (MHz)	η_Q	δ_σ (ppm)	η_σ	Euler angles		
						α	β	γ
Extended structures								
a3nii_ohside		-9.90 -11.6	0.192 0.272	-584.686 -582.857	0.157 0.166	22.7 22.9	14.2 13.8	-29.9 -29.9
a3nii_oxide		-9.89 -11.4	0.257 0.342	-562.091 -557.283	0.137 0.154	80.2 83.3	5.26 5.21	-49.3 -49.7
a3nn		-11.4 -13.1	0.0797 0.164	-563.858 -567.389	0.181 0.204	-77.6 -75.4	3.64 3.66	59.3 56.7
a3ncc		11.3 12.7	0.834 0.892	-422.846 -426.550	0.279 0.320	-88.3 -85.0	8.00 8.11	-64.8 -70.5
a3nnc		-9.23 -10.8	0.816 0.725	-434.907 -439.195	0.266 0.307	-8.06 -12.9	5.21 5.78	23.2 25.9
c5ni_eq		-12.4 -14.2	0.788 0.635	-526.775 -516.716	0.146 0.129	-68.6 -72.0	12.5 12.1	54.7 53.5
c5nii_eq		10.8 -12.2	0.917 0.895	-590.916 -583.478	0.113 0.148	-68.6 -68.5	9.10 9.14	60.2 60.3

Table 2 (Continued)

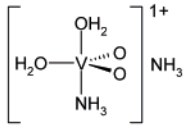
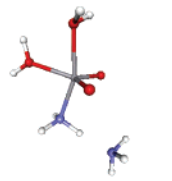
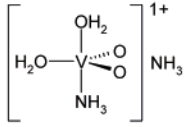
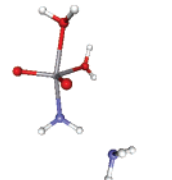
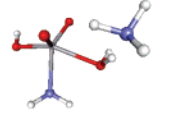
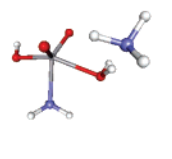
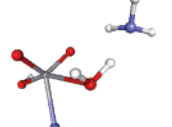
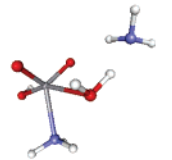
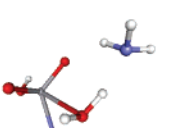
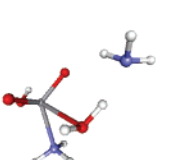
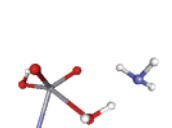
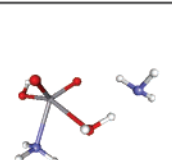
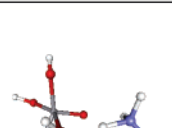
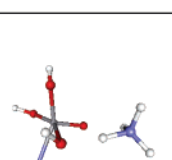
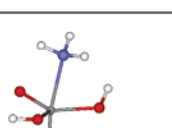
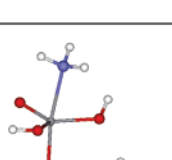
		C _Q (MHz)	η _Q	δ _σ (ppm)	η _σ	Euler angles		
						α	β	γ
Extended structures								
c6ni_eq 		8.80	0.877	-578.253	0.317	-48.7	0.0543	49.6
		11.0	0.783	-576.429	0.294	-48.2	0.0544	49.5
c6nii_eq 		9.18	0.862	-593.790	0.351	33.1	18.7	-39.4
		11.5	0.773	-594.861	0.331	32.6	18.9	-38.2
n2niii_eq_oxo_H2O 		-9.26	0.637	-516.927	0.260	10.8	10.6	8.35
		-11.0	0.716	-518.110	0.250	11.4	10.7	7.45
n2niv_ax_oxo_H2O 		-9.05	0.682	-526.400	0.279	41.7	16.5	-17.2
		-10.8	0.768	-525.526	0.269	42.0	16.4	-17.1
n2niv_eq_oxo_H2O 		-9.05	0.682	-526.400	0.279	41.7	16.5	-17.2
		-10.8	0.768	-525.526	0.269	42.0	16.4	-17.1
n2nv_ax_OH_H2O 		-9.03	0.633	-541.100	0.270	34.4	16.5	-20.7
		-10.8	0.725	-540.751	0.259	34.7	16.4	-21.0
n3cii_eq 		-6.49	0.933	-616.787	0.0377	6.23	16.2	-18.1
		-7.15	0.939	-615.681	0.0365	5.55	15.9	-17.9
n3ci 		-4.84	0.671	-544.575	0.166	35.5	11.9	-18.2
		-5.84	0.447	-534.014	0.177	35.9	11.5	-17.8

Table 2 (Continued)

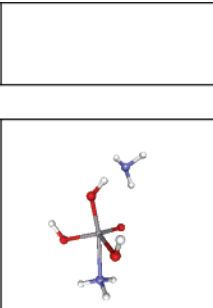
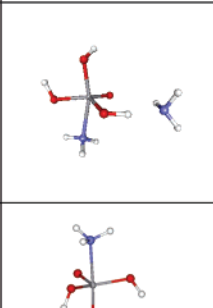
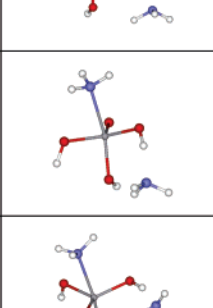
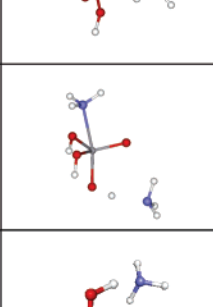
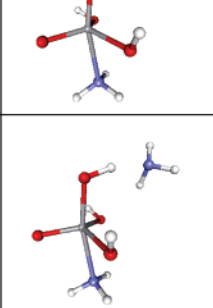
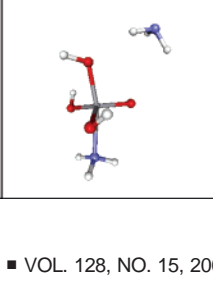

		C_Q (MHz)	η_Q	δ_σ (ppm)	η_σ	Euler angles		
						α	β	γ
Extended structures								
n3ni_ax_OH_don_oxo		-4.04	0.700	-429.222	0.230	-0.000426	7.61	0.0111
		-4.66	0.992	-425.833	0.233	-0.000667	7.59	0.0104
n3nii_eq_oxo_noHbondax		-5.86	0.736	-394.175	0.226	-15.6	3.11	70.6
		-7.05	0.616	-392.024	0.242	-16.5	3.02	67.1
n3niiiAX		-6.87	0.159	-544.840	0.240	46.3	8.27	-23.7
		-8.16	0.305	-541.677	0.253	45.5	8.07	-21.7
n3niiiEQ		-6.83	0.162	-544.371	0.238	46.2	8.10	-23.4
		-8.12	0.300	-541.616	0.252	45.3	7.91	-21.3
n3nii		-5.86	0.736	-394.175	0.226	-15.6	3.11	70.6
		-7.05	0.616	-392.024	0.242	-16.5	3.02	67.1
n3ni		-4.04	0.700	-429.222	0.230	-0.000426	7.61	0.0111
		-4.66	0.992	-425.833	0.233	-0.000667	7.59	0.0104
n3niv_ax		-4.66	0.467	-506.153	0.143	-12.1	11.1	20.0
		-5.45	0.723	-503.444	0.149	-11.3	11.0	19.4
n3niv_eq_ax		-4.66	0.466	-505.899	0.143	-12.1	11.1	20.0
		-5.45	0.722	-503.206	0.149	-11.3	11.0	19.4
n3nv_ax		-5.32	0.197	-574.770	0.148	-30.4	18.0	21.8
		-6.29	0.0809	-567.420	0.161	-30.1	17.7	21.3

Table 2 (Continued)

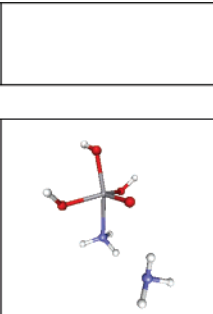
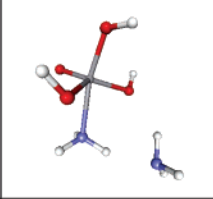
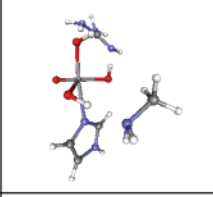
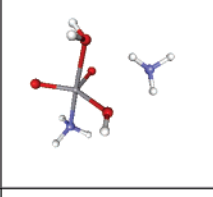
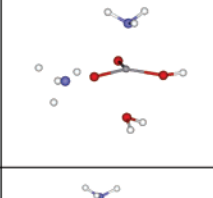
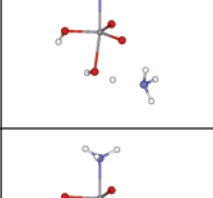
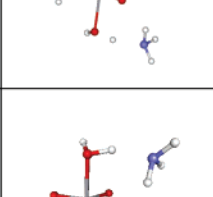
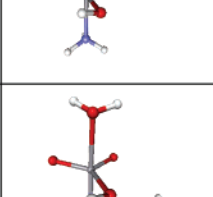
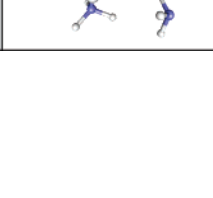
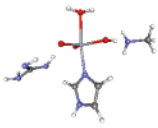
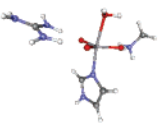
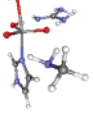
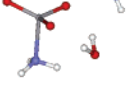
		C_Q (MHz)	η_Q	δ_σ (ppm)	η_σ	Euler angles		
						α	β	γ
Extended structures								
n3nvi_eq		-4.19	0.219	-586.402	0.108	-2.02	15.5	0.928
		-4.96	0.132	-583.359	0.113	-1.98	15.4	0.862
n3nvii_eq		-4.17	0.165	-596.984	0.0906	45.4	16.8	-35.0
		-4.91	0.147	-592.418	0.0994	45.3	16.6	-34.8
n3nn		-8.52	0.325	-482.173	0.185	-72.0	7.96	-81.3
		-9.89	0.227	-475.079	0.214	-73.1	7.84	-77.8
n5cii_eq		-13.8	0.268	-738.852	0.272	86.9	6.40	52.9
		-16.3	0.348	-736.719	0.315	87.4	6.25	52.2
n5ci		-13.6	0.836	632.339	0.226	17.7	10.4	-30.0
		-16.0	0.736	656.449	0.213	16.3	10.2	-30.0
n5ni_ax		-15.7	0.184	-612.430	0.145	-35.1	13.8	44.5
		-18.1	0.0987	-609.799	0.186	-34.3	13.7	44.1
n5ni_eq		-15.7	0.185	-612.293	0.145	-34.8	13.6	44.6
		-18.1	0.0998	-609.646	0.186	-34.0	13.5	44.1
n5nii_ax		-15.1	0.166	-658.129	0.0772	45.4	19.2	-47.1
		-17.5	0.147	-656.860	0.122	44.8	19.0	-46.6
n5niii_eq		-17.0	0.0741	-613.937	0.126	-35.2	16.9	35.7
		-19.5	0.0119	-614.329	0.151	-34.8	16.8	35.1

Table 2 (Continued)

		C_Q (MHz)	η_Q	δ_σ (ppm)	η_σ	Euler angles		
						α	β	γ
Extended structures								
n5nii		-16.9	0.220	-512.714	0.152	-5.54	3.81	44.6
		-19.1	0.162	-508.055	0.190	-6.03	3.74	49.9
n5nc		-16.2	0.386	-410.733	0.220	-49.8	6.07	-67.1
		-18.3	0.340	-408.878	0.252	-50.1	6.19	-66.5
n5nnii		-16.5	0.217	-508.721	0.158	-7.71	11.2	20.2
		-18.7	0.192	-508.122	0.196	-9.31	11.2	23.0
a4n		-16.8	0.164	-174.361	0.0387	-35.7	0.0730	61.2
		-19.3	0.180	-174.808	0.0649	-48.3	0.0727	72.0

^a Highlighted in bold are the structures for which the experimental and computed C_Q and δ_σ are in agreement. The top entries in each row are calculated with the TZV basis set, the bottom, with 6-311+G. The chemical structures of model compounds are shown in ball-and-stick representation. V atoms are small gray spheres; C, larger gray spheres; O, red; H, white; N, blue; K^+ ions, purple. Schematic representations are shown for the basic structures as well as for a3-, c5-, and c6-type structures whose calculated NMR parameters are in agreement with those experimentally determined.

NMR parameters in agreement with the experimental data. However, none of these structures are biologically relevant as vanadate is not in the trigonal bipyramidal geometry. Therefore, we conclude that these complexes do not represent meaningful resting state geometries.

Interestingly, calculated NMR parameters for an additional two models with overall cationic vanadate, **c5ⁿ_{i-ii}** and **c6ⁿ_{i-ii}**, are in agreement with the experimental results. These structures were considered biologically relevant but improbable due to their higher energies compared with the lower-energy overall neutral species.¹⁴ We speculate that, in VCPO, these geometries might be stabilized by the protein; however, at pH 8.0 it does not seem very likely that two equatorial oxygen atoms would be protonated as those in **c5**-type structures. Additional work is necessary to address these questions.

Our calculations additionally permitted us to rule out the **n3**- and **n5**-type structures as the plausible resting state geometries. It was proposed that if the vanadate were neutral, it would likely oscillate between these two structures.¹⁴ However, of the 11 **n3**-type and 10 **n5**-type complexes, only 1 (**n3ⁿⁿ**) showed any agreement with the experiment (Table 2). Both equatorial oxygens are protonated in this complex, and we speculate that at pH 8.0 this would be very unlikely.

An additional intriguing hypothesis has been put forth by Carlson, Pecoraro, and Kravitz¹⁷ based on the QM/MM calculations of the extended VCPO models: that the resting state is a

hybrid between the **a3**- and **a4**-type geometries (the latter containing an axial water ligand and three equatorial oxo groups). In the small active site models the **a4**-type structures are unstable resulting in the dissociation of the axial aqua-ligand, and therefore the calculations of the NMR parameters are meaningless. Much larger models are necessary to investigate whether the NMR observables for that geometry would resemble the experimental result; this work is computationally demanding and will be reported in a separate study.

It is also important to note that contrary to the anisotropic tensorial quantities, the computed ⁵¹V isotropic chemical shifts (Table 1s of the Supporting Information) do not exhibit any meaningful trends as a function of the coordination environment of the vanadate cofactor. This is not unexpected because isotropic chemical shifts are a complex function of the environment. It was also evident from our DFT calculations of isotropic shifts in model compounds which correlated poorly with the observed shifts. No meaningful chemical information about the metal environment in VCPO can therefore be extracted from the isotropic shifts alone. This reinforces the importance of determination of complete quadrupolar and chemical shift anisotropies by solid-state NMR.

Discussion

The catalytic mechanism of vanadium-containing haloperoxidases has been addressed by numerous experimental and,

very recently, computational investigations.^{5–8,10,11,14–17,38,53–63} A wealth of crucial information about many aspects of function of these enzymes has been gained from these studies. However, an experimental atomic-level picture of the coordination environment of the vanadate cofactor ultimately reporting on the catalytic activity has been unavailable until the current work, due to the limited resolution of the X-ray structures and lack of direct spectroscopic probes of the active vanadium(V) state. In this report, we establish that a combination of experimental ⁵¹V solid-state MAS NMR spectroscopy and quantum mechanical DFT calculations of the spectroscopic observables yield important insight regarding the coordination geometry of the vanadate in VCPO. Our results indicate that the most probable resting state of the protein under our experimental conditions involves an anionic vanadate cofactor with the axial hydroxo ligand, while one hydroxo and two oxo groups are present in the equatorial plane. This is in remarkable agreement with the DFT and QM/MM studies by Carlson, Pecoraro, and colleagues.^{14,17} However, two cationic geometries with the parent structures **c5** and **c6** might be feasible in which the axial ligand is either hydroxo or aqua, while the equatorial plane contains either one hydroxo and two oxo groups or one aqua and two hydroxo groups, respectively. These were considered improbable based on the energetic considerations, but whether they could be stabilized by the protein environment remains to be addressed. Exploring the intriguing possibility of the hybrid resting state oscillating between the **a3** and **a4** structures¹⁷ entails high-level QM/MM calculations of NMR observables using extended active site models.

Our results highlight the fact that quadrupolar interaction is typically dominated by the electronic charges within 4–5 Å from the nucleus, and therefore DFT calculations of the EFG tensor even for small active site models accurately predict the magnitude of the quadrupolar interaction. A protein environment is very important for providing long-range electrostatic interactions,¹⁷ and we hypothesize that its main role might be in forcing a particular set of protonation states on the vanadate oxygens. Solid-state NMR spectroscopy is a direct and sensitive probe of these protonation states in VCPO, as demonstrated in this work. We note that in a number of inorganic systems in solution the isotropic ⁵¹V NMR chemical shifts were found to be sensitive to the protonation states of the oxo functions directly attached to vanadium, as has been reported previously.^{64–66}

The sensitivity of the 14.1 T ⁵¹V SSNMR experiments with the current setup is such that we can extract the quadrupolar tensor elements with the precision of ca. 15%, which is somewhat lower than that in the bioinorganic model complexes (7–15%). On the other hand, the CSA tensor elements are determined with the same precision as that in the model compounds, due to the very high signal-to-noise ratio of the central transition region in the MAS spectra. Overall, this is sufficient for gaining indispensable chemical information: in conjunction with the quantum mechanical DFT calculations, ⁵¹V solid-state NMR measurements define the protonation states of the ligands in the vanadate cofactor; this information is not available from X-ray diffraction or other experimental approaches. It will be of interest soon to establish whether with the current approach the nature of the unprotonated oxygens could be established (i.e., doubly bonded V=O group could be distinguished from the oxo group V–O[–]); additional experimental and computational work will be required to address this question.

⁵¹V has to date found very limited use as a spectroscopic NMR probe of biological systems. In solution, it has been utilized to study metal ion binding to human apo-transferin^{67,68} and to probe vanadium binding to VBPO.⁶⁰ However, only isotropic chemical shifts are measured by solution NMR, limiting the information content of the spectra. It is clear from this study that, in order to gain atomic-level chemical information, knowledge of both quadrupolar and chemical shift tensors (rather than a single isotropic chemical shift value) is required. These two anisotropic interactions report on different, complementary aspects of the electronic and geometric structure. Prior to our work, no reports have appeared on ⁵¹V solid-state NMR spectroscopy in biological systems, despite the favorable NMR properties of the vanadium nucleus. The results reported in this manuscript establish ⁵¹V SSNMR spectroscopy as a direct and sensitive probe of the electronic and geometric structure of vanadium sites in proteins.

Conclusions

We have presented the first example of ⁵¹V solid-state NMR spectroscopy in a protein, a 67.5-kDa vanadium chloroperoxidase. The anisotropic NMR observables extracted from the numerical analysis of the spinning sideband manifold spanning the central and satellite transitions as well as from the central transition lineshape analysis provide the first direct experimental probe of the detailed coordination environment of the vanadate cofactor in the resting state of the protein. Quantum mechanical DFT calculations of the NMR parameters for an extensive series of VCPO active site models indicate that the vanadate cofactor is most likely anionic with one axial hydroxo ligand, one equatorial hydroxo-, and two equatorial oxo- groups. A combination of experimental solid-state NMR and quantum mechanical calculations thus offers a powerful strategy for analysis of a vanadium center in vanadium haloperoxidases. Our approach is expected to contribute to the fundamental understanding of the relationships between the electrostatic environment of the vanadium center and the catalytic activity in this

(53) Almeida, M.; Filipe, S.; Humanes, M.; Maia, M. F.; Melo, R.; Severino, N.; da Silva, J. A. L.; da Silva, J. J. R. F.; Wever, R. *Phytochemistry* **2001**, *57* (5), 633–642.

(54) Casny, M.; Rehder, D.; Schmidt, H.; Vilter, H.; Conte, V. *J. Inorg. Biochem.* **2000**, *80* (1–2), 157–160.

(55) Colpas, G. J.; Hamstra, B. J.; Kampf, J. W.; Pecoraro, V. L. *J. Am. Chem. Soc.* **1996**, *118* (14), 3469–3478.

(56) de Boer, E.; Wever, R. *J. Biol. Chem.* **1988**, *263* (25), 12326–12332.

(57) Martinez, J. S.; Carroll, G. L.; Tschirret-Guth, R. A.; Altenhoff, G.; Little, R. D.; Butler, A. *J. Am. Chem. Soc.* **2001**, *123*, 3289–3294.

(58) Messerschmidt, A.; Prade, L.; Wever, R. *Biol. Chem.* **1997**, *378* (3–4), 309–315.

(59) Ohshiro, T.; Littlechild, J.; Garcia-Rodriguez, E.; Isupov, M. N.; Iida, Y.; Kobayashi, T.; Izumi, Y. *Protein Sci.* **2004**, *13*, 1566–1571.

(60) Rehder, D.; Casny, M.; Grosse, R. *Magn. Reson. Chem.* **2004**, *42* (9), 745–749.

(61) Rehder, D.; Schulzke, C.; Dau, H.; Meinke, C.; Hanss, J.; Epple, M. *J. Inorg. Biochem.* **2000**, *80*, 115–121.

(62) Tanaka, N.; Dumay, V.; Liao, Q. N.; Lange, A. J.; Wever, R. *Eur. J. Biochem.* **2002**, *269* (8), 2162–2167.

(63) ten Brink, H. B.; Schoemaker, H. E.; Wever, R. *Eur. J. Biochem.* **2001**, *268*, 132–138.

(64) Buhl, M.; Parrinello, M. *Chem.—Eur. J.* **2001**, *7*, 4487–4494.

(65) Andersson, I.; Gorzsas, A.; Kerezsi, C.; Toth, I.; Pettersson, L. *Dalton Trans.* **2005**, 3658–3666.

(66) Pettersson, L.; Andersson, I.; Gorzsas, A. *Coord. Chem. Rev.* **2003**, *237*, 77–87.

(67) Butler, A.; Danzitz, M. J.; Eckert, H. *J. Am. Chem. Soc.* **1987**, *109*, 1864–1865.

(68) Butler, A.; Eckert, H. *J. Am. Chem. Soc.* **1989**, *111*, 2802–2809.

important class of enzymes and to be generally applicable to studies of diamagnetic vanadium sites in vanadium-containing proteins.

Acknowledgment. We thank our collaborator Professor Dieter Rehder for the generous gift of the model bioinorganic oxovanadium(V) complexes. T.P. acknowledges financial support of the University of Delaware, the National Science Foundation (NSF-CAREER CHE-0237612), the ACS Petroleum

Research Fund (PRF Grant No. 39827-G5M), and the National Institutes of Health (P20-17716 under COBRE program, and 2 P20 016472-04 under INBRE program of NCCR).

Supporting Information Available: DFT calculated NMR parameters for all active site models, results of nutation experiments, and full citation of ref 40. This material is available free of charge via the Internet at <http://pubs.acs.org> JA060480F